J. Fluid Mech. (1981), *vol.* 104, *pp.* 159–187
Printed in Great Britain

Wave-energy extraction by a submerged cylindrical resonant duct

By M. J. SIMON

Department of Applied Mathematics and Theoretical Physics, University of Cambridge

(Received 14 May 1980)

A cylindrical duct absorbing energy from incident surface waves is considered. The asymptotic properties of the scattering and radiation potentials are determined, to yield the hydrodynamic quantities on which the energy absorption characteristics of the duct can be shown to depend. It is shown that it is possible to tune the resonant response of the duct to absorb the maximum theoretical energy at a given frequency. Curves are presented showing the variation of energy absorption and the amplitude of the duct response with frequency for various depths of submergence and various tuning frequencies.

1. Introduction

In a recent paper in the *Journal of Fluid Mechanics*, Lighthill described analyses relevant to the absorption of wave energy by submerged resonant ducts, with particular reference to the programme being pursued by the Design and Projects Division of Vickers, Ltd. This programme is investigating a number of different design configurations based on the idea that submerged devices could more easily survive the effects of local storms than surface devices, and that a submerged device could extract a significant fraction of the incident power if designed to resonate at a suitable frequency and to have a broad enough frequency response. These ideas lead to the resonant duct, which has the added advantage that a device incorporating this principle has the minimum of moving parts, simply those associated directly with power take-off.

The original concept of the engineering design (Lighthill 1979), based on the resonant duct, has been modified for the reason that the large air volume that was needed to avoid a high pneumatic stiffness produced excessive structure and mooring costs. Also the need for rectification of the duct oscillations (which was originally achieved by an 'overtopping' system) is currently obviated in the design by using a Wells air-turbine. (This turbine has the interesting property that its direction of rotation is independent of the direction of the air flow.)

Thus the present design can be represented schematically in figure 1. The introduction of the mouth-downwards duct greatly reduces the pneumatic stiffness in the device, and allows a much more compact structure than the original concept. Also, the forcing pressure at the mouth of the downwards duct is much smaller than at the upwards duct, and so the hydrodynamic interaction of the device (when extracting energy or passive) with the incident ocean swell is principally just that of an upward-facing duct. It is this aspect of device performance which this paper is to describe.

0022-1120/81/4682-3760 $02.00

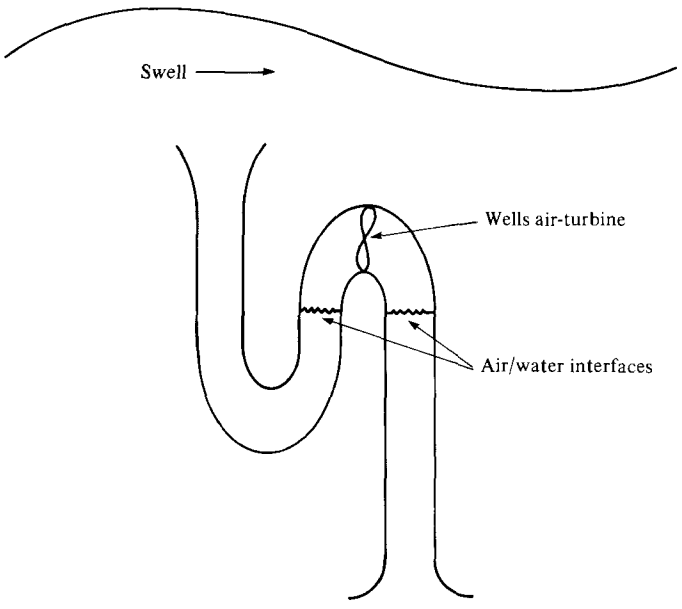

FIGURE 1. Schematic diagram of the Vickers twin oscillating water-column wave-energy device.

The analyses presented in Lighthill (1979) are two-dimensional, in that the device is thought of as being of very large dimension parallel to the wave crests; the very powerful tools of complex analysis can then be applied to give exact values for the important hydrodynamic quantities. Whereas this idealization may have much in common with a closely spaced row of discrete devices, and with tests of an isolated device in a narrow wave tank, there is much to be learned from an analysis for a single device; further, if a row of devices is envisaged where the spacing is comparable to the wavelength of the incident swell, then in order to study the interactions between devices it is useful to know, for example, the scattering of an incident wave from a single device.

Although an exact analysis of even the simplest truly three-dimensional configuration seems unattainable, it proved possible to extend the approximate variational technique of Evans & Morris (1972*a*, *b*) to solve the problem of the scattering from an idealized duct. This yields the scattering coefficients and the 'pressure-amplification factor'. The radiation potential (that is, the solution when there is no incident wave, and flow in the duct generates radiating waves) is simply related to the scattering potential by a reciprocal theorem (Newman 1962). This is pursued in §8, giving the 'radiation damping coefficient'. The 'added mass' is a combination of two terms, one of which is obtained in §9 using the Kramers–Kronig relations, and the other term, an infinite-frequency contribution, is obtained by inverting an integral equation in §10. Curves of the quantities which arise in the scattering and radiation problems are presented and discussed in §11, and using these results the energy absorption properties of the duct are computed and shown in §12, 13.

This whole analysis is performed for the case where the ocean is infinitely deep; strictly this is applicable provided the wavelength is less than about 3·5 times the ocean depth. The complementary study in finite depth is considered in Thomas

(1981), where the radiation problem is solved first, in contrast to the present paper. This solution yields the radiation damping and the added mass, and as expected these quantities agree with the present analysis in the limit as the depth becomes large. Thomas also uses the reciprocal theorem, but now to derive the exciting force, a property of the scattering problem equivalent to the pressure-amplification factor. This different method of solution is available in the finite-depth case because infinite matrix equations replace the integral equations solved here. The different character of the energy-absorption characteristics in his paper is due mainly to use of an adjustable spring constant instead of the (fixed) gravitational stiffness of the Vickers' device.

Part 1. The scattering problem

2. Formulation and statement of the problem

A circular duct of radius a is submerged a depth h under the surface of infinite fluid on which plane small-amplitude surface waves of a single frequency ω are propagating. The motion is assumed linear and irrotational. Axes (x, y, z) and (r, θ, z) are chosen, with z measured downwards from the undisturbed free surface, x and $\theta = 0$ being in the direction of wave propagation, so that the duct is modelled as $r = a$, $h \leqslant z < \infty$.

To start with, only the scattering of surface waves by the duct is considered; the potential due to an oscillating flow in the duct can be superposed later. Thus the condition that there is no flow at great depths in the duct can be imposed for the scattering problem.

Potentials will be written in the form

$$\mathrm{Re}\left[\frac{g\mathscr{A}}{\omega} e^{i\omega t}\,\Phi\right], \tag{1}$$

where $2\mathscr{A}$ is the crest-to-trough height of the waves. Thus the potential of waves incident from $x = -\infty$ is

$$\Phi^I = e^{-Kz - iKx} = e^{-Kz - iKr\cos\theta} \quad (K = \omega^2/g), \tag{2}$$

which can be split into partial waves as

$$\Phi^I = e^{-Kz}\left\{J_0(Kr) + 2\sum_{n=1}^{\infty}(-i)^n J_n(Kr)\cos(n\theta)\right\}, \tag{3}$$

where J_n is the Bessel function of order n (Abramowitz & Stegun 1964).

The form (3) suggests writing

$$\Phi = \Phi^I + \Phi^s = \phi_0 + 2\sum_{n=1}^{\infty}(-i)^n\phi_n, \tag{4}$$

where ϕ_n is proportional to $\cos(n\theta)$, and satisfies Laplace's equation in the fluid, with the free-surface condition, namely

$$\nabla^2\phi_n = 0 \tag{5a}$$

and

$$\left(\frac{\partial}{\partial z} + K\right)\phi_n = 0 \quad \text{on} \quad z = 0, \tag{5b}$$

together with the boundary conditions on the body, at large depth, and at the centre

$$\frac{\partial}{\partial r}\phi_n = 0 \quad \text{at} \quad r = a, \quad z > h; \tag{6a}$$

$$\phi_n \text{ and } \frac{\partial}{\partial r}\phi_n \text{ are continuous at } \quad r = a, \quad z < h; \tag{6b}$$

$$\phi_n \to 0 \quad \text{as} \quad z \to \infty \quad \text{for} \quad r > a; \tag{6c}$$

$$\phi_n \text{ is bounded at } \quad r = 0. \tag{6d}$$

To impose uniqueness on the solution there must be a radiation condition

$$\phi_n^s = \phi_n - J_n(Kr)\, e^{-Kz} \cos(n\theta) \sim \text{outgoing waves as} \quad r \to \infty. \tag{7}$$

Henceforward the problem for ϕ_n will be described as the 'nth mode', characterized by $\cos(n\theta)$ dependence. Solutions of (5a, b) are

$$e^{-Kz} H_n^{(1)}(Kr)\cos(n\theta), \quad e^{-Kz} H_n^{(2)}(Kr)\cos(n\theta) \tag{8a}$$

and

$$M(k,z)\, I_n(kr)\cos(n\theta), \quad M(k,z)\, K_n(kr)\cos(n\theta) \quad (k > 0), \tag{8b}$$

where $H_n^{(1)}$ and $H_n^{(2)}$ are Hankel functions which represent incoming and outgoing circular waves respectively, and

$$J_n(Kr) = \tfrac{1}{2} H_n^{(1)}(Kr) + \tfrac{1}{2} H_n^{(2)}(Kr) \tag{9}$$

is thus the r-dependence of a circular standing wave, with no net transport of energy radially. Also I_n, K_n are modified Bessel functions and $M(k,z)$, a function which satisfies the free-surface condition (5b), is given by

$$M(k,z) = k\cos(kz) - K\sin(kz). \tag{10}$$

The pair (8b) of solutions for any $k > 0$, represent disturbances local in r, and so a linear combination of such can be used to satisfy the boundary conditions at $r = a$. Thus $\phi_n \sec(n\theta)$ can be written

$$\{J_n(Kr) + A_n H_n^{(2)}(Kr)\}\, e^{-Kz} + \int_0^\infty B_n(k)\, K_n(kr)\, \frac{M(k,z)}{k(k^2+K^2)}\, dk \quad (r > a), \tag{11a}$$

$$C_n J_n(Kr)\, e^{-Kz} + \int_0^\infty D_n(k)\, I_n(kr)\, \frac{M(k,z)}{k(k^2+K^2)}\, dk \quad (r < a), \tag{11b}$$

where (7) has been used in the former relation; in the latter the condition of no net flow in the duct is implicit, and (6d) has been used.

It will be seen that A_n is the scattering amplitude of the nth mode, and C_n is effectively the amplitude of the standing wave in $r < a$; these quantities are determined with high accuracy by the variational technique described in the next section. Since the incident wave of the nth mode, $J_n(Kr)\, e^{-Kz}\cos(n\theta)$, constitutes an exact balance between incoming and outgoing energy flux, the full solution must have this feature also. Noting that (9) gives

$$J_n(Kr) + A_n H_n^{(2)}(Kr) = \tfrac{1}{2}[H_n^{(1)}(Kr) + (2A_n + 1) H_n^{(2)}(Kr)], \tag{12}$$

this requires

$$|2A_n + 1| = 1 \quad \text{for all } n. \tag{13}$$

The most important aspect of the scattering solution is the fact that it supplies the driving pressures for the motions in the duct from which energy is extracted. For a narrow duct (and, to a first approximation, for wider ducts) the amplitude of the driving pressure is simply the amplitude of the pressure fluctuations at the duct mouth; but in general will be this quantity multiplied by a factor K_A (complex to include modification of amplitude and phase). This driving pressure is just that found 'in the depths' of the duct, or in practice at least one duct diameter below the mouth. Hence K_A can be defined as

$$K_A = \frac{\text{excess pressure sensed in the depths of the duct}}{\text{excess pressure at } r = 0,\ z = h \text{ if the duct were absent}}, \tag{14}$$

where excess pressure means excess over the hydrostatic distribution. This factor is denoted by $K e^{-i\alpha}$ in Lighthill (1979) and is the most important result of the determination of the scattering potential.

The excess pressure is given by

$$p_e = -\rho i\omega\Phi, \tag{15}$$

(where ρ is the 'uniform' density of the ocean), and so

$$K_A = (\lim_{\substack{z\to\infty \\ r<a}} \Phi)/(\Phi^I \text{ at } r = 0,\ z = h) = e^{Kh} \lim_{\substack{z\to\infty \\ r<a}} \Phi. \tag{16}$$

Now, observing that any solution of Laplace's equation (5a) in a tube must average out across the tube at large distances along the length, and that the average of $\cos(n\theta)$ in $0 \leqslant \theta < 2\pi$ is zero for $n \geqslant 1$, (16) becomes

$$K_A = e^{Kh} \lim_{\substack{z\to\infty \\ r<a}} \phi_0 = e^{Kh} \phi_0^\infty, \quad \text{say.} \tag{17}$$

So only the $n = 0$ mode contributes to K_A. (Similarly in the radiation problem, the solution is independent of θ because the forcing volume flow must be.) It is thus fortunate that only this mode needs to be considered for K_A, and later for the radiation damping and added length (although for any future study of the interactions of devices all the A_n would be needed).

Henceforward only the $n = 0$ mode will be considered and the suffix will be dropped from A_0, $B_0(k)$, C_0 and $D_0(k)$.

From (11)

$$K_A = e^{Kh} \lim_{z\to\infty} \left\{ \int_0^\infty D(k)\, I_0(kr) \frac{M(k,z)}{k(k^2+K^2)}\, dk \right\}, \tag{18}$$

and it is expected that this limit exists and is independent of r. An extension to the variational method described in §6 provides a representation of this limit in terms of quantities calculated in §5, and the accuracy of this estimate is checked in §7.

3. The integral equations

The variational technique adopted here is not original; it was first used in the context of water waves by Miles (1967, 1971) and was used by Evans & Morris (1972a, b) to study reflection of surface waves by one or two plane vertical barriers, in cases of

normal and oblique incidence. The technique relies crucially on the following theorem, due to Havelock (1929), for inverting expressions such as (11a, b):
If

$$f(z) = A\,e^{-Kz} + \int_0^\infty B(k)\frac{M(k,z)}{k^2+K^2}\,dk, \tag{19}$$

is a suitably well-behaved function of $z \in (0,\infty)$, then

$$A = 2K\int_0^\infty f(t)\,e^{-Kt}\,dt, \tag{20a}$$

and

$$B(k) = \frac{2}{\pi}\int_0^\infty f(t)\,M(k,t)\,dt \quad (k > 0). \tag{20b}$$

In what follows, trial functions which are estimates for

$$F(z) = \frac{\partial\phi_0}{\partial r} \quad \text{at} \quad r = a \pm \epsilon, \quad G(z) = [\phi_0]_{a-\epsilon}^{a+\epsilon}, \tag{21}$$

will be used to obtain close upper and lower bounds for a real positive quantity ζ, defined below, from which A and C can be found.

From (11)

$$\left.\begin{aligned} F(z) &= -K\{J_1(\mu) + AH_1^{(2)}(\mu)\}\,e^{-Kz} - \int_0^\infty B(k)\,K_1(ka)\frac{M(k,z)}{k^2+K^2}\,dk \\ &= -KCJ_1(\mu)\,e^{-Kz} + \int_0^\infty D(k)\,I_1(ka)\frac{M(k,z)}{k^2+K^2}\,dk, \end{aligned}\right\} \tag{22}$$

where $\mu = Ka$, and so

$$J_1(\mu) + AH_1^{(2)}(\mu) = CJ_1(\mu) = -2\int_0^h F(t)\,e^{-Kt}dt, \tag{23a}$$

$$-B(k)\,K_1(ka) = D(k)\,I_1(ka) = \frac{2}{\pi}\int_0^h F(t)\,M(k,t)\,dt, \tag{23b}$$

since by (6a)

$$F(z) = 0 \quad (z > h). \tag{24}$$

Also

$$\begin{aligned} G(z) &= \{(1-C)\,J_0(\mu) + AH_0^{(2)}(\mu)\}\,e^{-Kz} + \int_0^\infty \{B(k)\,K_0(ka) - D(k)\,I_0(ka)\}\frac{M(k,z)}{k(k^2+K^2)}\,dk \\ &= -\frac{2iA}{\pi\mu J_1(\mu)}\,e^{-Kz} + \int_0^\infty \frac{B(k)}{k^2aI_1(ka)}\frac{M(k,z)}{k^2+K^2}\,dk, \end{aligned} \tag{25}$$

(using (23), and the known values of the Wronskians involved, to simplify the form), and so

$$\frac{-iA}{\pi\mu J_1(\mu)} = K\int_h^\infty G(t)\,e^{-Kt}dt, \tag{26a}$$

$$\frac{B(k)}{k^2aI_1(ka)} = \frac{2}{\pi}\int_h^\infty G(t)\,M(k,t)\,dt, \tag{26b}$$

since by (6b)

$$G(z) = 0 \quad (z < h). \tag{27}$$

Substituting (26*b*) into (22) and using (24) gives

$$\int_0^h F(t)\,S^-(t,z)\,dt = -\frac{iA}{\pi\mu J_1(\mu)}\,e^{-Kz} \quad (z < h), \tag{28}$$

where

$$S^-(t,z) = \int_0^\infty [k(k^2+K^2)\,\bar{H}(ka)]^{-1}\,M(k,t)\,M(k,z)\,dk, \tag{29}$$

with

$$\bar{H}(x) = 2xI_1(x)\,K_1(x) \tag{30}$$

and the kernel $S^-(t,z)$ contains a logarithmic singularity at $t = z$.

Note that

$$\left.\begin{aligned} \bar{H}(x) &> 0 \quad \text{for all} \quad x > 0, \\ &\to 1 \quad \text{as} \quad x \to \infty, \\ &\sim x \quad \text{as} \quad x \to 0. \end{aligned}\right\} \tag{31}$$

Similarly, substituting $B(k)$ from (23*a*) into (25), and using (27) gives

$$\int_h^\infty G(t)\,S^+(t,z)\,dt = -\pi KCJ_1(\mu)\,e^{-Kz} \quad (z > h), \tag{32}$$

where

$$S^+(t,z) = \lim_{\delta\to 0}\int_0^\infty e^{-k\delta}\,\frac{k\bar{H}(ka)}{k^2+K^2}\,M(k,t)\,M(k,z)\,dk, \tag{33}$$

where the exponential forces convergence of the integral.

It is conjectured that $F(z)$, $G(z)$ each has constant phase (cf. Garrett 1970); if a solution can be found using this assumption, then it is the only solution, by virtue of the uniqueness which imposition of the radiation condition (7) produces. Moreover, it can be shown that the integral equations (28) and (30) have unique solutions when conditions (24) and (27) are applied.

Writing

$$F(z) = \frac{-iA}{2\mu J_1(\mu)}f(z) \quad \text{and} \quad G(z) = -\pi KCJ_1(\mu)\,g(z), \tag{34}$$

(28) and (23*a*) become

$$\int_0^h f(t)\,S^-(t,z)\,dt = e^{-Kz} \quad (z < h), \tag{35a}$$

$$\int_0^h f(t)\,e^{-Kt}\,dt = \zeta, \tag{35b}$$

while (32), (26*a*) give

$$\int_h^\infty g(t)\,S^+(t,z)\,dt = e^{-Kz} \quad (z > h), \tag{36a}$$

$$\int_h^\infty g(t)\,e^{-Kt}\,dt = (\pi^2K^2\zeta)^{-1}, \tag{36b}$$

where

$$\zeta = \frac{C}{iA}\,\mu J_1^2(\mu). \tag{37}$$

It was previously stated that ζ is real; it is easily seen that this is self-consistent with (13), (23*a*) and with $f(z)$, $g(z)$ being real. It is shown that ζ is also positive in the next section.

4. The variational approach

A dual-extremum principle will be constructed from (35) and (36) which will yield close bounds for ζ when trial functions $\chi(z)$, $\psi(z)$ are used to approximate $f(z)$, $g(z)$.

Note that

$$\int_0^h \int_0^h l(t)\, l(z)\, S^-(t,z)\, dt\, dz = \int_0^\infty [k(k^2+K^2)\,\bar{H}(ka)]^{-1} \left(\int_0^h l(t)\, M(k,t)\, dt \right)^2 dk \geqslant 0, \quad (38)$$

for all real functions $l(z)$, and replacing $l(z)$ by $f(z)$ shows that $\zeta \geqslant 0$. Then if $\chi(z)$ approximates the shape of $f(z)$, take

$$l(z) = f(z) - \frac{\zeta \chi(z)}{\int_0^h \chi(t)\, e^{-Kt}\, dt}, \quad (39)$$

which, with (35), gives

$$\mathscr{L}^-[\chi] = \frac{\int_0^\infty [k(k^2+K^2)\,\bar{H}(ka)]^{-1} \left(\int_0^h \chi(t)\, M(k,t)\, dt \right)^2 dk}{\left(\int_0^h \chi(t)\, e^{-Kt}\, dt \right)^2} \geqslant \frac{1}{\zeta}. \quad (40)$$

Thus the functional $\mathscr{L}^-$ is an upper bound to $1/\zeta$ for all functions $\chi(z)$; and, if $\chi(z)$ models the shape of $f(z)$ to within $O(\epsilon)$ (so that $l(z)$ is this order), then $\mathscr{L}^-[\chi]$ is greater than $1/\zeta$ by an amount that is $O(\epsilon^2)$, and ζ can, as a result, be estimated closely using somewhat crude trial functions. $\mathscr{L}^-$ is also invariant under a scale transformation of $\chi(z)$.

Similarly from (36), with $\psi(z)$ approximating the shape of $g(z)$,

$$\mathscr{L}^+[\psi] = \frac{\int_0^\infty (k^2+K^2)^{-1}\, k\bar{H}(ka) \left(\int_h^\infty \psi(t)\, M(k,t)\, dt \right)^2 dk}{\left(\int_h^\infty \psi(t)\, e^{-Kt}\, dt \right)^2} \geqslant \pi^2 K^2 \zeta, \quad (41)$$

which provides an upper bound for ζ.

5. Choice of trial functions

It is desirable to minimize both $\mathscr{L}^-[\chi]$ and $\mathscr{L}^+[\psi]$ to obtain bounds for ζ that are close, which will be the case if χ, ψ contain the essential behaviour of f, g. Recalling that potential flow near a sharp lip has square-root behaviour suggests that the properties

$$(h-z)^{\frac{1}{2}}\chi(z) \quad \text{and} \quad (z-h)^{-\frac{1}{2}}\psi(z) \quad \text{are bounded near} \quad z = h, \quad (42)$$

must be incorporated into the trial functions.

It also proves convenient to form $\bar{\chi}(z)$, $\bar{\psi}(z)$, where

$$\bar{\chi}\left(\frac{z}{h}\right) = \chi(z) - K\int_z^h \chi(t)\, dt, \quad \bar{\psi}\left(\frac{z}{h}\right) = h\left(\frac{d}{dz}+K\right)\psi(z). \quad (43)$$

By (42), both $\overline{\chi}(z)$ and $\overline{\psi}(z)$ should have inverse square-root singularities at $z = 1$. The reason for the formation of $\overline{\chi}$, $\overline{\psi}$ can most easily be seen if the limit is considered as the duct radius becomes large; in this limit the scattering resembles the problem of normal incidence on a single vertical barrier for which the exact solution of Ursell (1947) exists, giving (to within multiplicative constants)

$$\overline{\chi}(z) = (1-z^2)^{-\frac{1}{2}} \quad (0 < z < 1), \quad \overline{\psi}(z) = (z^2-1)^{-\frac{1}{2}} \quad (z > 1). \tag{44}$$

The functionals $\mathscr{L}^-$ and $\mathscr{L}^+$ can be rewritten in terms of $\overline{\chi}$, $\overline{\psi}$ respectively using

$$\int_0^h \chi(t)\, M(k,t)\, dt = kh \int_0^1 \overline{\chi}(t) \cos(kht)\, dt, \tag{45a}$$

$$\int_0^h \chi(t)\, e^{-Kt} dt = h \int_0^1 \overline{\chi}(t) \cosh(Kht)\, dt, \tag{45b}$$

$$\int_h^\infty \psi(t)\, M(k,t)\, dt = -\int_1^\infty \overline{\psi}(t) \sin(kht)\, dt - \psi(h) \sin(kh), \tag{45c}$$

$$\int_h^\infty \psi(t)\, e^{-Kt} dt = \frac{1}{2K} \int_1^\infty \overline{\psi}(t)\, e^{-Kht} dt, \tag{45d}$$

and (42) implies that $\psi(h) = 0$.

The bounds (40) and (41) then become

$$\zeta \leqslant \zeta^+ = \int_0^\infty \left[\overline{H}\left(\frac{l}{\sigma}\right)\right]^{+1} \left(\int_1^\infty \overline{\psi}(p) \sin(lp)\, dp\right)^2 \frac{l\, dl}{l^2+\tau^2} \Big/ \left(\frac{\pi}{2} \int_1^\infty \overline{\psi}(p)\, e^{-\tau p}\, dp\right)^2, \tag{46a}$$

$$\frac{1}{\zeta} \leqslant \frac{1}{\zeta^-} = \int_0^\infty \left[\overline{H}\left(\frac{l}{\sigma}\right)\right]^{-1} \left(\int_0^1 \overline{\chi}(p) \cos(lp)\, dp\right)^2 \frac{l\, dl}{l^2+\tau^2} \Big/ \left(\int_0^1 \overline{\chi}(p) \cosh(\tau p)\, dp\right)^2, \tag{46b}$$

where $\tau = Kh$, and $\sigma = h/a = \tau/\mu$.

Although Evans & Morris (1972*a*, *b*) used simply (44), in their associated scattering problems, certain features of the present problem result in poor accuracy if no improvement is made to the trial functions. Thus use was made of

$$\overline{\chi}(z) = (1-z^2)^{-\frac{1}{2}} + \beta_1 + \gamma_1 z \quad (0 < z < 1), \tag{47a}$$

$$\overline{\psi}(z) = (z^2-1)^{-\frac{1}{2}} + \beta_2 + \gamma_2 z^{-1} \quad (1 < z < \infty). \tag{47b}$$

The bounds (46) are then in terms of integrals of tabulated functions, and are ratios of quadratic polynomials of the β_i, γ_i, which can then be optimized, independently, to obtain very close bounds for ζ. Even without the γ_i present the bounds for ζ are never more than 2 % apart for sensible values of the parameters τ and μ. The γ_i are introduced to provide the best estimate possible of the pressure amplification factor, K_A, derived in the next section.

Having found ζ (or close estimates for it), A and C are determined simply; (13) gives

$$A = -i\, e^{-i\alpha} \sin(\alpha), \tag{48a}$$

so

$$\arg(C) = \arg(iA) = -\alpha \tag{48b}$$

and

$$\frac{\zeta}{\mu J_1^2(\mu)} = \left|\frac{C}{A}\right| = \cot\alpha - \frac{Y_1(\mu)}{J_1(\mu)}. \tag{48c}$$

This phase angle α will be also shown to be the phase lag of the pressure-amplification factor $K_A = Ke^{-i\alpha}$ in the notation of Lighthill (1979).

6. The estimate for K_A

Equations (18), (23) and (34) give

$$K_A = -\frac{iAe^{\tau}}{\pi\mu J_1(\mu)} \lim_{z\to\infty} \int_0^h f(t)\, R(t,r,z)\, dt, \tag{49}$$

where

$$R(t,r,z) = \int_0^{\infty} \frac{I_0(kr)}{I_1(ka)} \frac{M(k,t)\, M(k,z)}{k(k^2+K^2)}\, dk$$

$$= \tfrac{1}{2}\,\mathrm{Re}\left(\frac{\partial}{\partial t} - K\right) \int_{-\infty}^{\infty} \frac{I_0(kr)}{I_1(ka)} \frac{\sin(kt)\, e^{ikz}}{k(k-iK)}\, dk, \tag{50}$$

and it is expected that $R(t,r,\infty)$ exists and is independent of r. Evaluating the principal-value integral (50) by closing the contour in the upper half k plane, and taking the limit as $z\to\infty$, the only contribution that remains is from the pole at $k = 0$, so

$$R(t,r,\infty) = \left(\frac{\partial}{\partial t} - K\right)\left(-\frac{\pi t}{\mu}\right) = \frac{\pi}{\mu}(Kt-1), \tag{51}$$

and this is indeed independent of r. Hence

$$K_A = -\frac{iA\, e^{\tau}}{\mu^2 J_1(\mu)} \int_0^h (Kt-1) f(t)\, dt. \tag{52}$$

The main difficulty with this extension to the variational method is that the shape of the function $f(z)$ can be closely matched by varying β_1, γ_1 to obtain the best lower bound for ζ, but the function is still determined only to $O(\epsilon)$. Using (39) gives

$$K_A = \frac{iAe^{\tau}}{\mu^2 J_1(\mu)} \left\{ \frac{\zeta \int_0^h (1-Kt)\, \chi(t)\, dt}{\int_0^h e^{-Kt} \chi(t)\, dt} + \int_0^h (1-Kt)\, l(t)\, dt \right\}, \tag{53}$$

and the second term in the bracket would be expected to be $O(\epsilon)$. The numerical evidence in § 7 suggests, however, that the errors are actually of smaller order than this and the estimate taken is thus

$$K_A = \frac{iA\zeta}{\mu^2 J_1(\mu)} \frac{\int_0^h (1-Kt)\, \chi(t)\, dt}{\int_0^h e^{-Kt} \chi(t)\, dt}$$

$$= Ce^{\tau} \left(\frac{J_1(\mu)}{\mu}\right) \frac{\int_0^1 \bar{\chi}(p)\, dp}{\int_0^1 \bar{\chi}(p) \cosh(\tau p)\, dp}. \tag{54}$$

Thus K_A has the phase of C which, by (48), is just $-\alpha$.

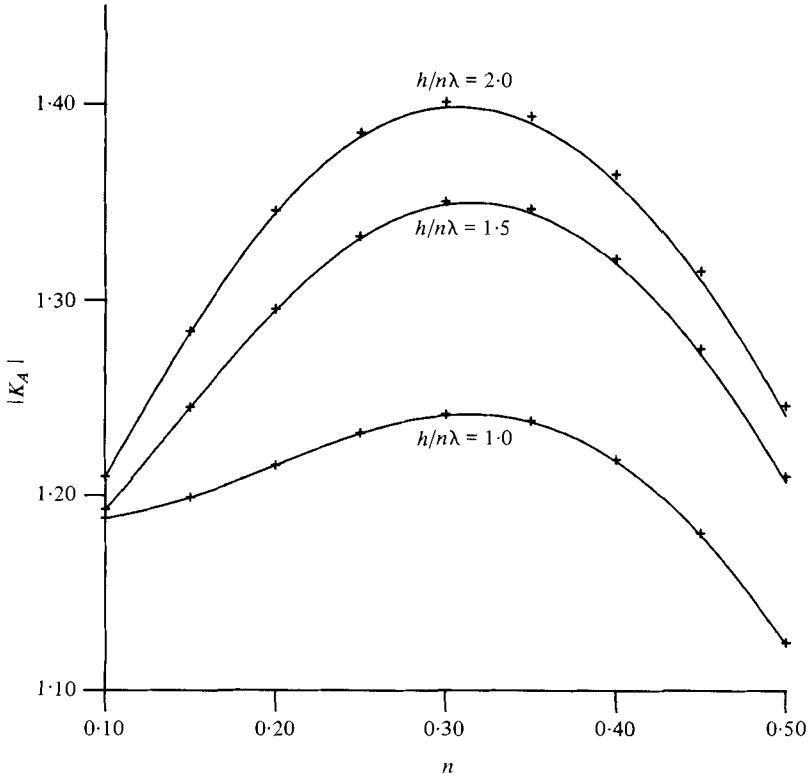

FIGURE 2. A comparison between the results for the pressure amplification factor $|K_A|$ given by the exact theory of Lighthill (1979), and the approximate technique employed in the present paper, adapted to the two-dimensional duct of width $n\lambda$. (Lighthill denotes this amplification factor by K.) Curves, exact theory; +, the corresponding approximate values.

Trial function	$\|K_A\|$	ζ	$\|C\|$	$\|A\|$
$\chi(p) = (1-p^2)^{-\frac{1}{2}}$	1·213778	1·477197	1·284690	0·168409
$\chi(p) = (1-p^2)^{-\frac{1}{2}} + \alpha_1$ (optimized)	1·161869	1·516126	1·275945	0·162968
$\chi(p) = (1-p^2)^{-\frac{1}{2}} + \alpha_1 + \beta_1 p$ (optimized)	1·160975	1·516822	1·275793	0·162874
$\psi(p) = (p^2-1)^{-\frac{1}{2}} + \alpha_2 + \beta_2 p^{-1}$ (optimized)	—	1·516999	1·275754	0·162850

TABLE 1. A comparison of estimates for $|K_A|$, ζ, $|C|$, $|A|$ using different trial functions for parameter values $\mu = \tau = 1{\cdot}0$.

7. A check on the accuracy of the estimate for K_A

The variational approach can be adapted to the two-dimensional problem for which the exact solution exists (Lighthill 1979). Equally well, this approach could be regarded as an extension of Evans & Morris (1972*b*, symmetric part), except that the barriers occupy $h < z < \infty$ instead of $0 \leqslant z < h$. The estimate is obtained from (54) by considering the symmetric part of the incident wave, which involves replacing $J_1(\mu)$ by $\sin(\mu)$ and dividing by 2 (since the symmetric part is only half the incident wave). Here μ denotes $K \times (\frac{1}{2}$ duct width$) = \pi n$ when the duct width is $n\lambda$. Figure 2

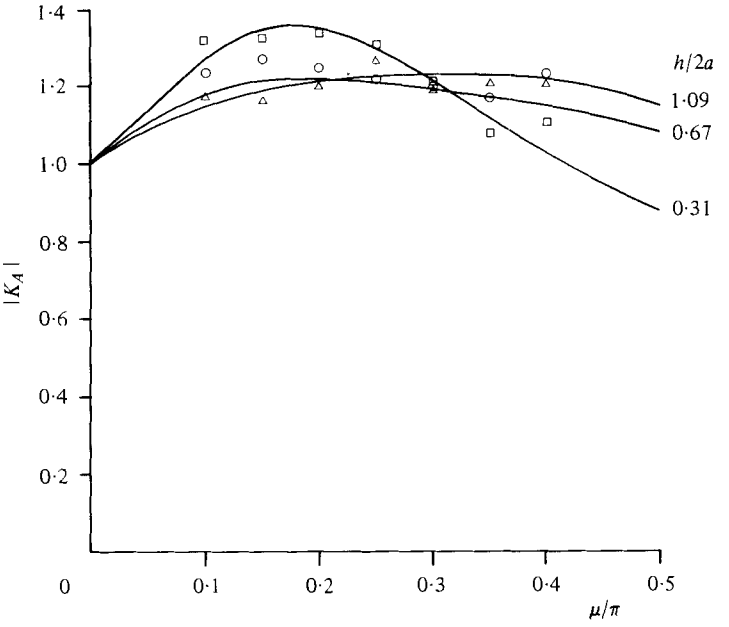

FIGURE 3. A comparison between the results for the pressure-amplification factor $|K_A|$ given by the variational technique of §6, and the experiments of Knott & Flower (1980), for different values of the ratio of mouth depth to duct radius. Curves, present theory; ×, $h/a = 0{\cdot}62$; ○, $h/a = 1{\cdot}34$; △, $h/a = 2{\cdot}18$.

shows the approximations and the exact value (given by equations (154a) and (165) of Lighthill 1979) for $0{\cdot}1 \leqslant n \leqslant 0{\cdot}5$ and different aspect ratios $h/n\lambda$. The agreement is clearly excellent.

Another check on the accuracy of (54) was to compare errors of the estimate for K_A with those of ζ, C, A as shown in table 1. Examination of the figures (which are typical of the values at different τ, μ) suggests that K_A has $O(\epsilon^2)$ errors, just as ζ, A, C do.

Finally, figure 3 shows experimental values determined in the wide wave tank at Edinburgh compared with the values predicted by this theory (Knott & Flower 1980). The experiments show a good agreement with theory, and confirm the qualitative behaviour of the pressure amplification, in that $|K_A| > 1$ in general, and with the largest values occurring for ducts near the surface.

This all suggests that (54) (with 47a) is a good estimate of K_A, and all further work is based upon it. Results of computations of C, A, and K_A are displayed in §11.

Having spent considerable time on one aspect of duct/swell interaction, when there is no flow in the duct, it is now possible to proceed to the situation where there is no incident wave but there is an oscillating flow in the duct. Later the two solutions can be suitably superposed to model a real duct extracting energy from incident waves.

Part 2. The radiation problem

8. The reciprocal theorem

The potential due to an oscillating flow

$$\mathrm{Re}\left[\frac{g\mathscr{A}}{\omega}\,Q\,e^{i\omega t}\right] \tag{55}$$

is sought. Without performing a complete solution to the problem, it is possible to use information from the scattering problem to determine the behaviour of the potential in the far field and in the depths of the duct. This is achieved by using Green's theorem, which gives

$$I[\Phi_1, \Phi_2] = \int_{\mathscr{S}} \left\{\Phi_1 \frac{\partial \Phi_2}{\partial n} - \Phi_2 \frac{\partial \Phi_1}{\partial n}\right\} dS = 0, \tag{56}$$

for any suitably well-behaved harmonic functions Φ_1, Φ_2 defined in and on a closed surface $\mathscr{S}$. For this application of the theorem, $\mathscr{S}$ is taken as the free surface, a cylindrical closure of large radius R, the fluid bottom at $z = \infty$, and the walls of the duct.

Assuming that Φ_1, Φ_2 satisfy the free surface condition (5*b*), and the boundary condition on the body and at large depth (6*a*, *c*), then the only contributions to (56) are from the cylindrical closure at $r = R$ and from the depths of the duct. Hence

$$\pi a^2 \left[\Phi_1 \frac{\partial \Phi_2}{\partial z} - \Phi_2 \frac{\partial \Phi_1}{\partial z}\right]_{\substack{z \gg h \\ r < a}} + 2\pi R \int_0^\infty \left[\Phi_1 \frac{\partial \Phi_2}{\partial r} - \Phi_2 \frac{\partial \Phi_1}{\partial r}\right]_{r=R} dz = 0, \tag{57}$$

assuming that at least one of Φ_1, Φ_2 is independent of θ.

This will be applied to

Φ_1 = scattering potential of $n = 0$ mode,

Φ_2 = radiation potential due to an oscillating flow $\mathrm{Re}\left[\frac{g\mathscr{A}}{\omega}\,Q\,e^{i\omega t}\right]$.

That is

$$\Phi_1 \sim \{J_0(Kr) + AH_0^{(2)}(Kr)\}\,e^{-Kz} \quad \text{as} \quad r \to \infty, \tag{58a}$$

$$\Phi_1 \sim e^{-\tau} K_A \quad \text{as} \quad z \to \infty \quad \text{for} \quad r < a, \tag{58b}$$

and

$$\Phi_2 \sim \hat{B} H_0^{(2)}(Kr)\,e^{-Kz} \quad \text{as} \quad r \to \infty, \tag{59a}$$

$$\Phi_2 \sim -\frac{Q}{\pi a^2}(z - a\hat{C}) \quad \text{as} \quad z \to \infty \quad \text{for} \quad r < a. \tag{59b}$$

The dimensionless constants $\hat{B}$, $\hat{C}$ must be determined; application of (57) immediately gives

$$\hat{B} = \tfrac{1}{2} i K\, e^{-\tau} Q K_A, \tag{60}$$

which is equivalent to a source strength Q' at $r = 0$, $z = h$ in the absence of the duct where

$$\hat{B} = \tfrac{1}{2} i K\, e^{-\tau} Q' \tag{61a}$$

(from Thorne 1953), and so

$$Q' = QK_A. \tag{61b}$$

This demonstrates the well-known *reciprocity* between the radiation and scattering problems:

$$\frac{\text{the effective source strength at } r = 0,\ z = h \text{ in the absence of the duct}}{\text{the source strength in the depths of the duct}}$$

$$= \frac{\text{the excess pressure in the depths of the duct}}{\text{the excess pressure at } r = 0,\ z = h \text{ in the absence of the duct}}.$$

The volume flow (55) in the duct radiates energy away at a rate $(g\mathscr{A}/\omega)^2 E_r$, where

$$E_r = \frac{\rho\omega}{K}|\hat{B}|^2 = \tfrac{1}{4}\rho\omega K e^{-2\tau}|K_A Q|^2. \tag{62}$$

Defining the dimensionless radiation damping coefficient D_r such that the oscillating flow radiates energy away at a rate given by

$$E_r = \tfrac{1}{4}\rho\omega K D_r |Q|^2, \tag{63}$$

we see that

$$D_r = e^{-2\tau}|K_A|^2. \tag{64}$$

Another application of (57) to

$$\Phi_1^* = \Phi_2 = \text{radiation potential due to the oscillating flow,}$$

gives

$$\frac{|Q|^2}{\pi a}(\hat{C} - \hat{C}^*) = \frac{4i|\hat{B}|^2}{K}$$

or

$$\operatorname{Im}\hat{C} = \tfrac{1}{2}\pi\mu D_r. \tag{65}$$

9. The Kramers–Kronig relation

It only remains to determine $\operatorname{Re}\hat{C}$. This part can be written

$$\operatorname{Re}\hat{C} = \frac{h}{a} - \hat{l}, \tag{66a}$$

where

$$a\hat{l} = \text{effective added length of duct.} \tag{66b}$$

$\hat{l}$ is a dimensionless 'added-mass' term, due to the inertial response of the mass of water outside the duct.

The potential (59*b*), with (65) and (66), becomes

$$\Phi \sim -\frac{Q}{\pi a}\left[\left(\frac{z-h}{a}\right) + \hat{f}(\omega)\right], \tag{67a}$$

where

$$\hat{f}(\omega) = \hat{l}(\omega) - i\frac{\pi a}{2g}\omega^2 D_r(\omega). \tag{67b}$$

Now the system that produces a potential $\mathrm{Re}[(g\mathscr{A}/\omega)\,\Phi e^{i\omega t}]$ from an oscillating flow $\mathrm{Re}[(g\mathscr{A}/\omega)\,Q e^{i\omega t}]$ is clearly *causal* (and linear by the initial formulation), and so $\hat{f}(\omega)$ must be analytic in the lower half-plane, $\mathrm{Im}\,\omega < 0$. As a result $\hat{f}(\omega)$ satisfies

$$\hat{f}(\omega_0)-\hat{f}(\infty) = \frac{i}{\pi}\fint_{-\infty}^{\infty} \frac{\hat{f}(\omega)-\hat{f}(\infty)}{\omega-\omega_0}\,d\omega \tag{68}$$

(since physical considerations suggest that $\hat{f}(\omega)$ tends to a finite real limit as $|\omega|\to\infty$). Taking the real part gives the Kramers–Kronig relation

$$\mathrm{Re}\hat{f}(\omega_0)-\mathrm{Re}\hat{f}(\infty) = -\frac{1}{\pi}\fint_{-\infty}^{\infty} \frac{\mathrm{Im}\hat{f}(\omega)}{\omega-\omega_0}\,d\omega. \tag{69}$$

Now (63) implies that D_r is an odd function of ω since E_r is necessarily positive; hence (67) and (69) give

$$\hat{l}(\omega_0)-\hat{l}(\infty) = \frac{a}{g}\fint_0^{\infty} \frac{\omega^3 D_r(\omega)}{\omega^2-\omega_0^2}\,d\omega \tag{70}$$

or

$$\hat{l}(\mu_0)-\hat{l}(\infty) = \frac{1}{2}\fint_0^{\infty} \frac{\mu D_r(\mu)}{\mu-\mu_0}\,d\mu, \tag{71}$$

with quantities expressed as functions of $\mu = a\omega^2/g$. This can be used very easily to generate values of $\hat{l}(\mu_0)-\hat{l}(\infty)$ for a given duct configuration (that is, for a given $\sigma = h/a$), since D_r contains the factor $e^{-2r} = e^{-2\sigma\mu}$, so the integral can in practice be truncated at $\mu = 3/\sigma$. Results of such a computation are displayed in § 11.

10. The infinite-frequency added-length problem

Note that $\hat{l}(\mu_0)$ is still not completely determined since $\hat{l}(\infty)$ is required first. It turns out that $\hat{l}(\infty)$ is irrelevant for the frequency response of the duct in capturing energy, when the duct is assumed 'tuned' to a given frequency; but that it does affect the length of duct necessary for such a tuning.

The infinite-frequency problem is one where the free-surface condition becomes

$$\phi = 0 \quad \text{on} \quad z = 0, \tag{72}$$

with the result that the added mass is half that of the associated anti-symmetric problem where the duct operates together with its mirror image in the free surface. The duct flows are in anti-phase and the far field is thus of dipole type.

Write the infinite-frequency radiation potential as

$$\left.\begin{aligned} \phi &= \frac{Q}{\pi a^2}\int_0^{\infty} B(k)\,K_0(kr)\,\frac{\sin(kz)}{k}\,dk \quad (r > a) \\ &= -\frac{Q}{\pi a^2}\left\{z + \int_0^{\infty} D(k)\,I_0(kr)\,\frac{\sin(kz)}{k}\,dk\right\} \quad (r < a), \end{aligned}\right\} \tag{73}$$

and the quantity desired from the problem is

$$\hat{l}(\infty) = \frac{h}{a} - \frac{1}{a}\lim_{z\to\infty}\left(\frac{\pi a^2}{Q}\,\phi + z\right). \tag{74}$$

By a similar process to that used in §3, an integral equation can be formed in terms of

$$F(z) = \frac{\pi a^2}{Q} \frac{\partial \phi}{\partial r}\bigg|_{r=a},$$

and (74) can be manipulated as in the derivation of K_A to give

$$\hat{l}(\infty) = \frac{h}{a} - \frac{2}{a^2}\int_0^h tF(t)\,dt \tag{75a}$$

and

$$\int_0^h F(t)\,\bar{S}(t,z)\,dt = \frac{\pi}{2}z \quad (0 < z < h), \tag{75b}$$

with

$$\bar{S}(t,z) = 2\int_0^\infty \frac{\sin(kt)\sin(kz)}{k\bar{H}(ka)}\,dk \tag{75c}$$

and $\bar{H}$ as in (31). $\bar{S}(t,z)$ can be written

$$\bar{S}(t,z) = \ln\left|\frac{t+z}{t-z}\right| + \frac{1}{a}\int_0^\infty \frac{\sin(kt)\sin(kz)}{k^2}\,\bar{h}(ka)\,dk, \tag{76a}$$

where

$$\bar{h}(x) = 2x\left(\frac{1}{\bar{H}(x)} - 1\right) = (I_1(x)\,K_1(x))^{-1} - 2x, \tag{76b}$$

and the second term of $\bar{S}(t,z)$ is not singular at $t = a$.

The method adopted for the solution of (75) is essentially a Fourier decomposition. Differentiating (75b) with respect to z gives

$$\int_0^h F(t)\left\{\frac{2t}{t^2-z^2} + \frac{1}{a}\int_0^\infty \frac{\sin(kt)\cos(kz)}{k}\,\bar{h}(ka)\,dk\right\}dt = \frac{\pi}{2} \quad (0 < z < h), \tag{77}$$

or

$$\int_0^{\frac{1}{2}\pi} \cos\theta\,F(h\sin\theta)\left\{\frac{2\sin\theta}{\sin^2\theta - \sin^2\alpha} + \sigma\int_0^\infty \frac{\sin(l\sin\theta)\cos(l\sin\alpha)}{l}\,\bar{h}\left(\frac{l}{\sigma}\right)dl\right\}d\theta = \frac{\pi}{2}, \tag{78}$$

where t has been replaced by $h\sin\theta$, z by $h\sin\alpha$, h/a by σ, and kh by l in the inner integral. Now $F(t)$ has an inverse square-root singularity at $t = h$ and so $\cos\theta\,F(h\sin\theta)$ is bounded as $\theta \to \pi/2$. This suggests writing

$$\cos\theta\,F(h\sin\theta) = \sum_{r=1}^{\infty} a_r \sin(2r-1)\theta, \tag{79}$$

where all cosines are omitted since $F(t)$ is odd, and all even sines are omitted since it is conjectured that no part of $F(t)$ is regular at $t = h$. Making use of the results

$$\int_0^{\pi/2} \sin(2r-1)\theta\,\frac{2\sin\theta}{\sin^2\theta - \sin^2\alpha}\,d\theta = \pi\,\frac{\cos(2r-1)\alpha}{\cos\alpha} \tag{80a}$$

and

$$\int_0^{\pi/2} \sin(2r-1)\theta\sin(l\sin\theta)\,d\theta = \frac{\pi}{2}J_{2r-1}(l), \tag{80b}$$

gives

$$\sum_{r=1}^{\infty} a_r\left[\frac{\cos(2r-1)\alpha}{\cos\alpha} + \frac{\sigma}{2}\int_0^\infty \cos(l\sin\alpha)\frac{J_{2r-1}(l)}{l}\,\bar{h}\left(\frac{l}{\sigma}\right)dl\right] = \tfrac{1}{2}. \tag{81}$$

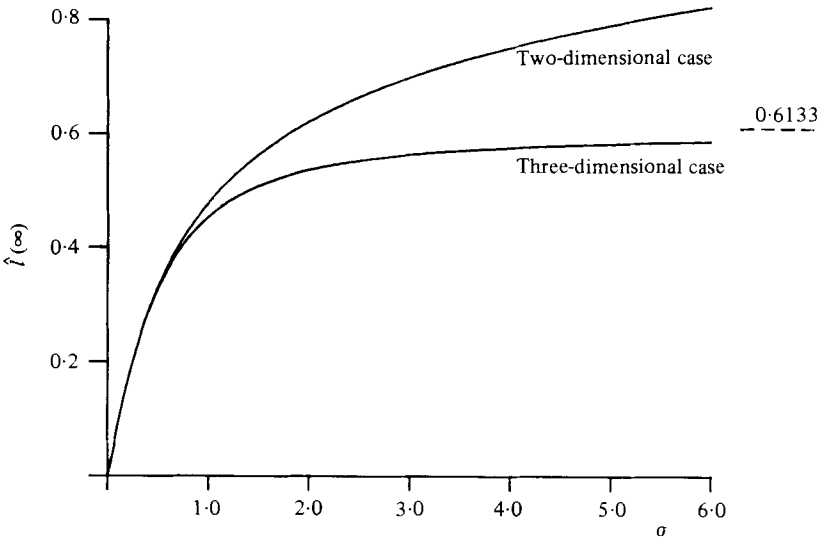

FIGURE 4. The infinite-frequency added-length coefficient $\hat{l}(\infty)$ plotted as a function of the aspect ratio σ. For the three-dimensional case the mouth depth and added length of duct are $a\sigma$ and $a\hat{l}(x)$ respectively (for duct radius a), whereas they are $d\sigma$ and $d\hat{l}(x)$ for the two-dimensional case, where d is the duct width. Dashed line, asymptotic value for the three-dimensional case as $\sigma \to \infty$.

Multiplying by $\cos\alpha \cos(2s-1)\alpha$ and integrating gives

$$\sum_{r=1}^{\infty} a_r \left[\delta_{rs} + \sigma(2s-1)\int_0^{\infty} l^{-2} J_{2r-1}(l) J_{2s-1}(l)\, \bar{h}\left(\frac{l}{\sigma}\right) dl\right] = \tfrac{1}{2}\delta_{1s}. \tag{82}$$

Here the results

$$\int_0^{\pi/2} \cos(2r-1)\alpha \cos(2s-1)\alpha\, d\alpha = \frac{\pi}{4}\delta_{rs} \tag{83a}$$

and

$$\int_0^{\pi/2} \cos\alpha \cos(2s-1)\alpha \cos(l\sin\alpha)\, d\alpha = \frac{\pi}{2}(2s-1)\frac{J_{2s-1}(l)}{l} \tag{83b}$$

are used. Thus the integral equation becomes the simultaneous linear equation (82), and can be written

$$(\hat{\mathbf{I}} + \mathbf{B})\,\mathbf{a} = \tfrac{1}{2}\mathbf{e}_1 \tag{84}$$

where $\mathbf{e}_1$ is a vector with 1 in the first place and zeroes elsewhere, $\mathbf{B}$ is the symmetric matrix with components

$$B_{rs} = \sigma \int_0^{\infty} \frac{J_{2r-1}(l) J_{2s-1}(l)}{l^2}\, \bar{h}\left(\frac{l}{\sigma}\right) dl, \tag{85}$$

and $\hat{\mathbf{I}}$ is diagonal with elements, $1, \frac{1}{3}, \frac{1}{5}, \frac{1}{7}, \ldots$.

Note that (75a) and (79) imply

$$\hat{l}(\infty) = \sigma - \frac{\pi}{2}\sigma^2 a_1. \tag{86}$$

The first component a_1 of $\mathbf{a}$ is given to high accuracy even when the infinite matrix $\mathbf{B}$ is replaced by a mere 3×3 one, which gives a value differing by less than 10^{-6} from the result using a 7×7 truncation, for all σ up to 6.

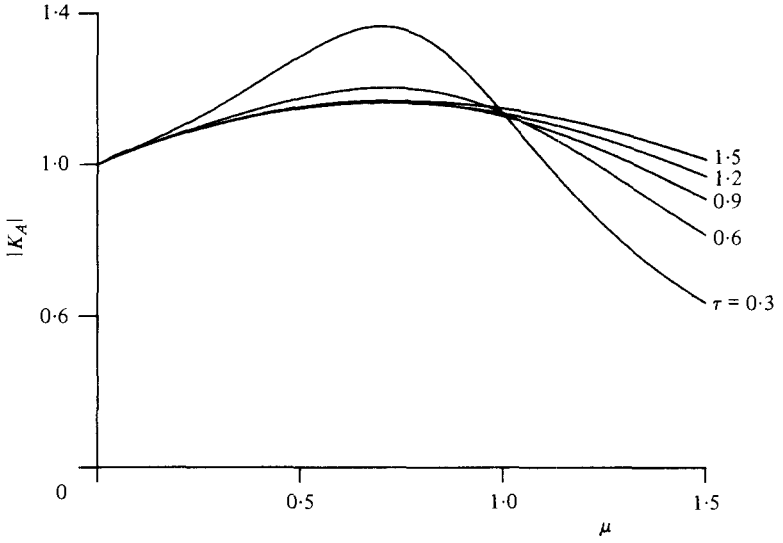

FIGURE 5. The pressure-amplification factor $|K_A|$ plotted as a function of the dimensionless wavenumber $\mu = Ka$ for different values of the dimensionless depth $\tau = Kh$.

Figure 4 shows $\hat{l}(\infty)$ plotted against $\sigma = h/a$; and for comparison the two-dimensional infinite frequency added length is also shown, although here σ represents $h/n\lambda$ = depth/duct width. For the two-dimensional case exactly the same analysis can be applied with $\bar{h}(x)$ replaced by

$$\bar{h}_2(x) = \frac{2x}{e^x - 1}. \tag{87}$$

The result of this calculation is indistinguishable in figure 4 from a computation of the exact value (using (114) and (174) of Lighthill 1979), which confirms the accuracy of the method. There is little qualitative difference between the curves except that the two-dimensional values are somewhat larger. As $\sigma \to \infty$, the three-dimensional added length is seen to be tending asymptotically to $0{\cdot}6113a$, the value given by Noble (1958) for the added length of an open pipe in infinite fluid, which is appropriate in this limit as the pipe moves away from the influence of the free surface.

11. Results from the scattering and radiation problems

The main points to emphasize here are the ways in which similarities and differences arise between the three-dimensional results and the two-dimensional exact solution of Lighthill (1979).

Consider then the pressure-amplification factor $|K_A|$, shown in figure 5, plotted against μ for different values of τ. This is equivalent to Lighthill, figure 6. A striking difference is revealed in that small immersion depths result in considerably enhanced amplifications over a significant range of values of μ; also, at greater than a certain depth the amplification becomes fairly insensitive to changes of depth or radius. This has important consequences for the design of a resonant-duct wave-energy device. These differences are also carried over to figure 6, which shows the radiation damping

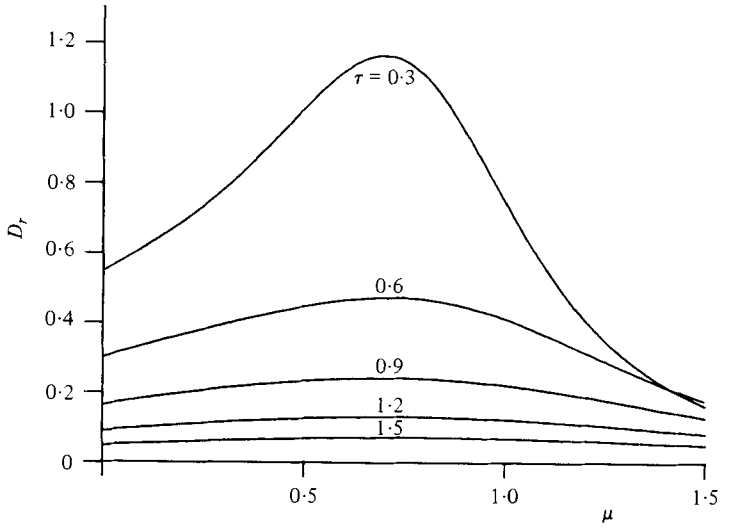

FIGURE 6. The radiation damping coefficient D_r plotted as a function of the dimensionless wavenumber $\mu = Ka$ for different values of the dimensionless depth $\tau = Kh$.

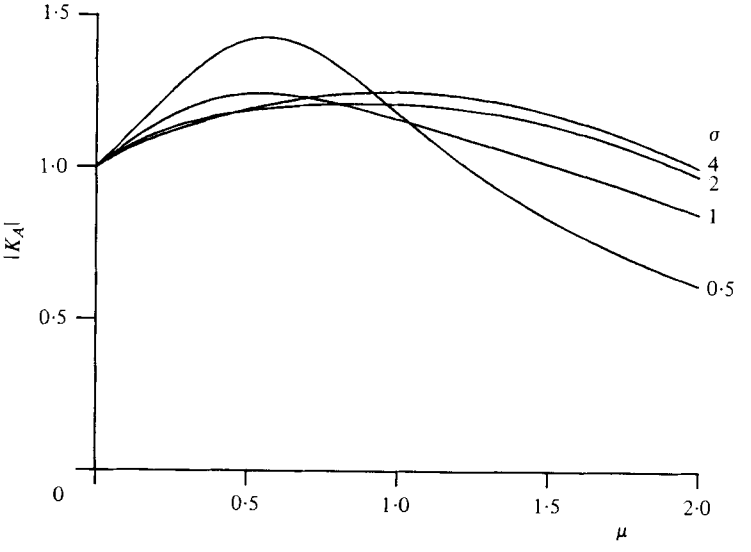

FIGURE 7. The pressure-amplification factor $|K_A|$ plotted as a function of the dimensionless wavenumber $\mu = Ka$ for different values of the aspect-ratio $\sigma = h/a$.

coefficient D_r computed from the curves of figure 5 using (64), for comparison with Lighthill, figure 13.

Strictly speaking figures 5–10 represent a single bound on the quantities involved, but the numerical evidence of table 1 demonstrates that the errors between bounds are not detectable graphically.

Figures 7 and 8 show $|K_A|$ and D_r plotted against $\mu = Ka$ for different values of the aspect-ratio $\sigma = h/a$. (This represents a given device in monochromatic seas of varying frequency.) For larger aspect ratios the amplification varies much less with

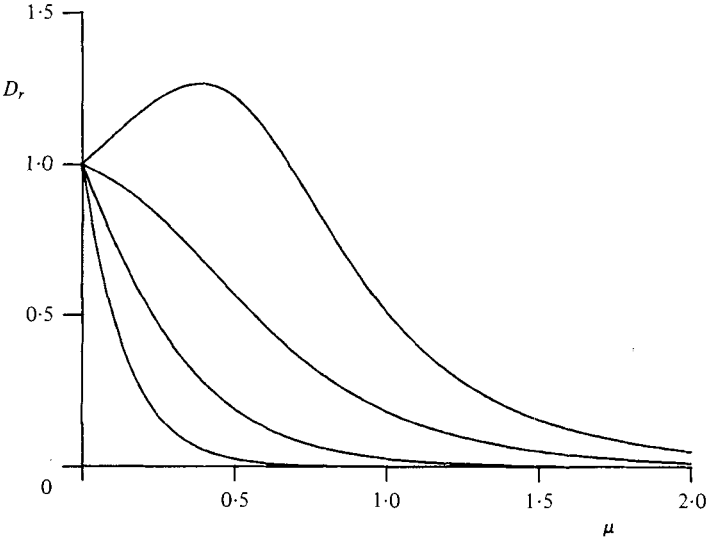

FIGURE 8. The radiation damping coefficient D_r plotted as a function of the dimensionless wavenumber $\mu = Ka$ for different values of the aspect ratio $\sigma = h/a$.

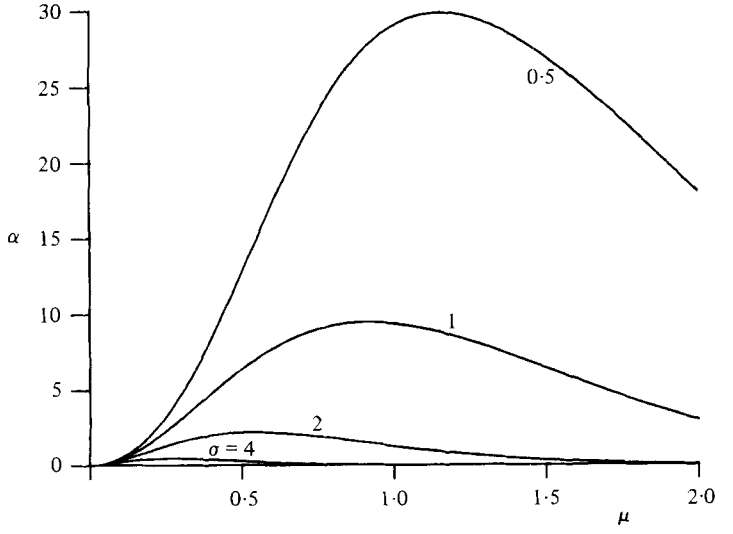

FIGURE 9. The phase angle α plotted against the dimensionless wavenumber $\mu = Ka$ for different aspect ratios. The quantities C, K_A and iA all have phase $-\alpha$, and A has modulus given by $\sin \alpha$.

μ than in the two-dimensional case (cf. Lighthill, figure 8). Also the very rapid decay of D_r with increasing frequency is the reason why the Kramers–Kronig relation (71) is so easy to put into practice.

For the sake of completeness, figures 9 and 10 present the phase angle α and the standing-wave amplitude $|C|$, plotted for different aspect ratios. Notice that α is

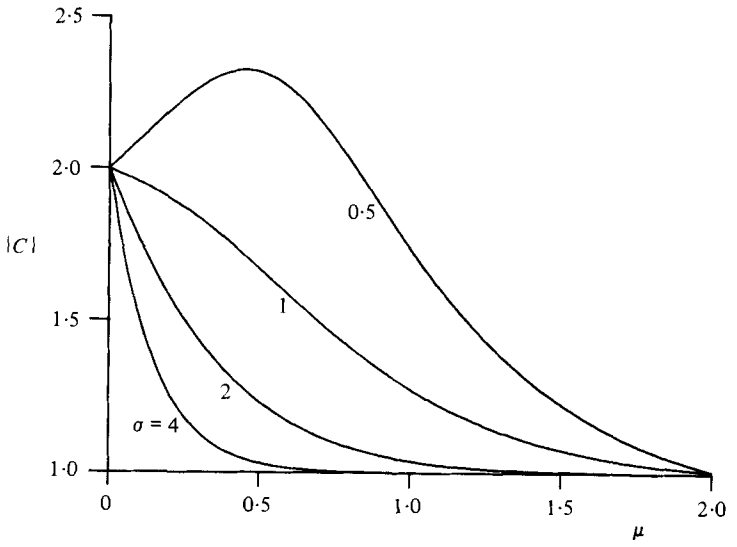

FIGURE 10. The modulus of the standing wave inside the duct, $|C|$, plotted against the dimensionless wavenumber $\mu = Ka$ for different aspect ratios.

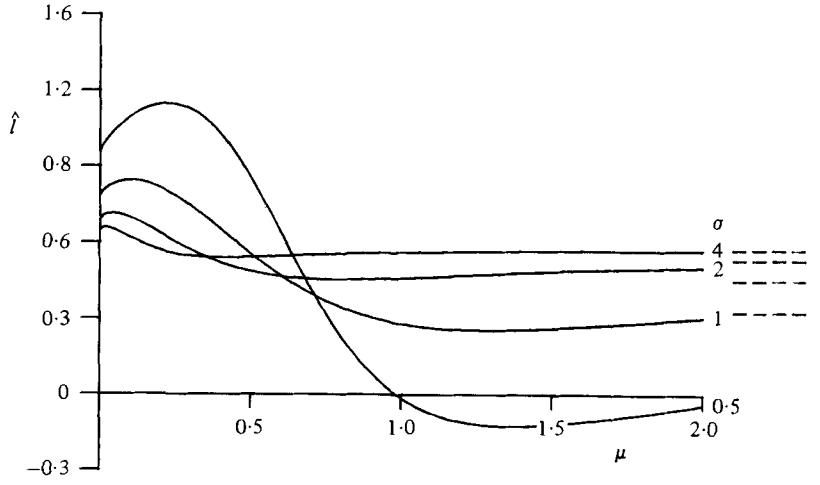

FIGURE 11. The added-length coefficient $\hat{l}$ plotted against the dimensionless wavenumber $\mu = Ka$ for different aspect ratios. Dashed lines: the infinite-frequency values given by the method of § 10.

always small and positive, as with the two-dimensional case, and that $(|C| - 1)$ bears a striking resemblance to D_r, although this seems to be coincidence.

The major difference between two- and three-dimensions occurs in considering the added lengths. For in two dimensions the added length is nearly always less than its infinite-frequency value, except very close to zero frequency, where it tends to *positive infinity, logarithmically*. Examination of figure 11 shows that there is a wide range of frequencies over which the added length is greater than the infinite-frequency value. Furthermore, this difference is large, particularly at fairly small values of σ

which the computations of §12 suggest would be appropriate for a real wave-energy device.

Another contrast in three dimensions is that the zero-frequency limit gives finite added length, which can be understood in terms of the source-type far field which arises in this limit, whereas the two-dimensional source implies a fluid flow with logarithmically infinite kinetic energy. These differences can also be seen as consequences of the Kramers–Kronig relations (see Kotik & Mangulis 1962). Again, there are important consequences here in terms of device design, since the resonant frequency and the bandwidth of the frequency response both depend on the added length. It is exactly the variation with frequency of the large added length which allows the system to respond well to frequencies away from resonance. By contrast, a system with nearly constant inertia and stiffness is dominated at low frequencies by the stiffness, at high frequencies by the inertia, and only near resonance is there a balance between the two opposing trends; for a good bandwidth this balance must be nearly satisfied over a wide range of frequencies. The resonant duct has fixed (gravitational) stiffness, and so it is necessary to employ the variation of the inertia, specifically using regions where the added length decreases with frequency.

Part 3. The resonant duct as a wave-energy absorber

12. Power absorption, tuning and bandwidth

Combining (58*b*) and (67) gives

$$\Phi \sim e^{-\tau} K_A - \frac{Q}{\pi a^2}(z-h+a\hat{l}-\tfrac{1}{2}i\pi a^2 K D_r) \tag{88}$$

and so

$$p_e \sim -\rho i\omega e^{-\tau} K_A + \rho\omega Q\left(\tfrac{1}{2}KD_r + i\left\{\frac{z-h+a\hat{l}}{\pi a^2}\right\}\right) \quad (z\to\infty, \quad r<a). \tag{89}$$

Consider now an upwards duct in the form of a U-tube of constant cross-sectional area πa^2 (half of the device pictured schematically in figure 1), where the curve of the U-bend is wide, and where the internal air–water interface is a distance Z measured along the duct from the mouth. On linear theory the oscillating flow (55) in the duct causes pressure fluctuations

$$\mathrm{Re}\left[\frac{g\mathscr{A}}{\omega} p_e e^{i\omega t}\right],$$

where

$$p_e = -\frac{\rho g Q}{i\omega\pi a^2} = -\frac{\rho\omega Q}{iK\pi a^2}, \tag{90}$$

at the interface; any 'pneumatic stiffness' is negligible because of the influence of the mouth-downwards duct. Equating (90) to the value of (89) at $z-h=Z$ gives

$$\rho i\omega e^{-\tau} K_A = \rho\omega Q\left(\tfrac{1}{2}KD_r + i\left\{\frac{Z+a\hat{l}-K^{-1}}{\pi a^2}\right\}\right). \tag{91}$$

As yet no energy extraction has been incorporated into the model; by analogy with (63) an energy extraction coefficient D_e is introduced such that energy is extracted at a rate

$$\tfrac{1}{4}\rho\omega K\left(\frac{g\mathscr{A}}{\omega}|Q|\right)^2 D_e \tag{92}$$

from the volume flow (55), as though the energy take-off process is strictly linear. Then (91) becomes

$$ie^{-\tau}K_A = Q\left\{\tfrac{1}{2}K(D_r+D_e)+\frac{i}{\pi a^2}(Z+a\hat{l}-K^{-1})\right\}. \tag{93}$$

Here any frictional losses are neglected; in practice a suitably rounded duct mouth would be needed to improve the device performance in larger-amplitude waves, since otherwise frictional dissipation (proportional to the cube of the amplitude) would dominate.

The energy extraction rate (92) is then

$$\tfrac{1}{4}\rho\omega K D_e\left(\frac{g\mathscr{A}}{\omega}\right)^2\left[D_r\Big/\left\{\tfrac{1}{4}K^2(D_e+D_r)^2+\left(\frac{Z+a\hat{l}-K^{-1}}{\pi a^2}\right)^2\right\}\right], \tag{94}$$

where (64) has been used to eliminate K_A. Thus every feature of the scattering problem has disappeared from the energy absorption characteristics of the device. The response is seen to depend only on D_r and $\hat{l}$ which are features of the radiation problem.

The incident energy flux is

$$\tfrac{1}{4}\rho\omega\left(\frac{g\mathscr{A}}{\omega}\right)^2 \tag{95}$$

(measured in watts per metre of frontage), and so the duct effectively captures energy over a frontage C_W given by

$$KC_W = \frac{D_e D_r}{\tfrac{1}{4}(D_e+D_r)^2+(Z/a+\hat{l}-1/\mu)^2/\pi^2\mu^2}. \tag{96}$$

For a given duct configuration, in seas of a given frequency ω_0 (and so K, μ, τ, D_r and $\hat{l}$ are fixed), (96) can be maximized to unity by

$$\left.\begin{aligned}&\frac{Z}{a}+\hat{l}-\frac{1}{\mu}=0\\&D_e=D_r\end{aligned}\right\}\quad \text{at}\quad \mu=\mu_0=a\omega_0^2/g. \tag{97a, b}$$

The former condition is that of resonance, that the amplitude of the volume-flow fluctuations determined by (93) should be a maximum; the latter condition equates the capture of energy and the radiation of energy in new waves.

The maximum of C_W is thus

$$\frac{1}{K_0}=\frac{\lambda_0}{2\pi}, \tag{98}$$

as predicted by Evans (1976) for any axisymmetric device with one vertical degree of freedom. At frequencies other than the resonant frequency, C_W is given by

$$KC_W = \frac{D_r(\mu_0)\,D_r(\mu)}{\tfrac{1}{4}(D_r(\mu_0)+D_r(\mu))^2+(1/\mu_0-\hat{l}(\mu_0)+\hat{l}(\mu)-1/\mu)^2/\pi^2\mu^2}, \tag{99}$$

if conditions (97) are applied and the coefficient D_e is a constant.

The device will be most cost-effective if it captures energy over a width as large as, or greater than, its diameter, and so considerable attention is focused on the quantity

$$\frac{C_W}{2a}=\frac{1}{2\mu}KC_W, \tag{100}$$

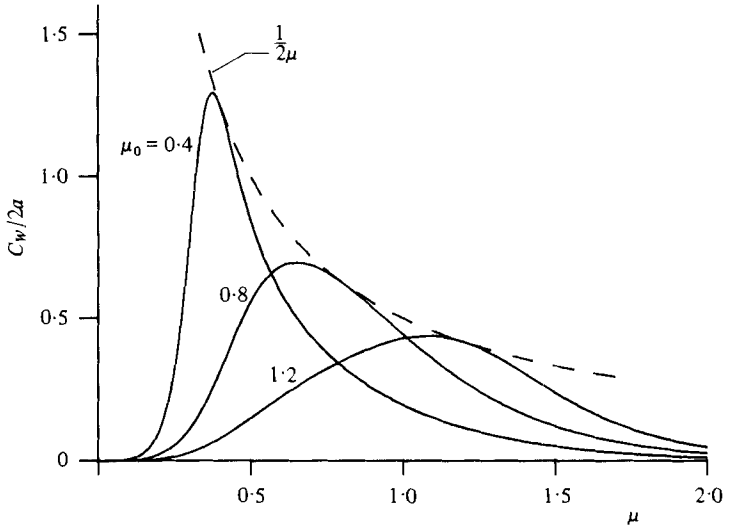

FIGURE 12. The ratio of capture width to duct diameter plotted against dimensionless wavenumber $\mu = Ka$ for a duct of aspect ratio $\sigma = 1{\cdot}0$, for different values of tuning wavenumber $\mu_0 = K_0 a$. Dashed curve: the maximum capture width to diameter ratio $1/2\mu$.

which is maximized under (97) to

$$1/2\mu_0, \tag{101}$$

and this tends to suggest that the device should be tuned to smallish values of μ_0. To compare the effect of different tuning frequencies, values $\mu_0 = 0{\cdot}4$, $0{\cdot}8$, $1{\cdot}2$ were used at a variety of different aspect ratios $\sigma = h/a$, and the results displayed in the next section.

Also of interest is the ratio between the amplitude of the response of the internal air/water interface, and the amplitude of the incident waves, given by

$$\left(\frac{g\mathscr{A}}{\omega}\right)\left(\frac{|Q|}{\omega\pi a^2}\right)\Big/\mathscr{A} = \frac{|Q|}{\pi a\mu}, \tag{102}$$

because the linear theory is not strictly admissible should this quantity exceed, say, 3.

It is worth noting at this stage that under the assumptions already made it is possible to incorporate a gradual taper or anti-taper into the duct, as in Lighthill (1979). Thus if the duct mouth still has radius a, but the cross-sectional area at a distance s from the mouth is

$$A(s) = A(0)/f(s) = \pi a^2/f(s), \tag{103}$$

then $(Z + a\hat{l} - K^{-1})$ can be replaced by

$$\int_0^Z f(s)\,ds + a\hat{l} - K^{-1}f(Z), \tag{104}$$

in equations (91), (93), (94), (96) and (97). Also the second term in the denominator of (99) becomes

$$\left(\frac{f(Z)}{\mu_0} - \hat{l}(\mu_0) + \hat{l}(\mu) - \frac{f(Z)}{\mu}\right)^2 \Big/ \pi^2\mu^2 \tag{105}$$

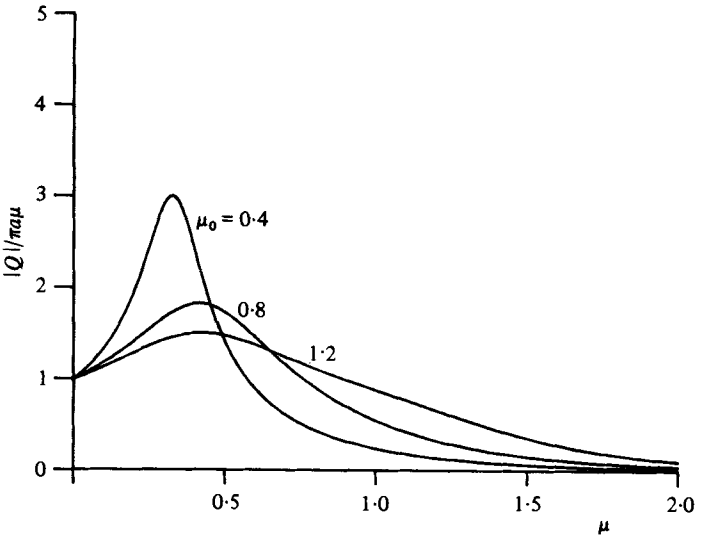

FIGURE 13. The ratio of the amplitude of the response in the duct to the wave height plotted against dimensionless wavenumber $\mu = Ka$ for a duct of aspect ratio $\sigma = 1{\cdot}0$, for different values of tuning wavenumber $\mu_0 = K_0 a$.

and the amplitude ratio (102) becomes

$$|Q|f(Z)/\pi a\mu. \tag{106}$$

It is clear from (105), (106) that the value of $f(Z)$ is crucial to the performance of the device, whereas the actual form of $f(s)$ in between the mouth and the air/water interface, only modifies the duct length necessary for the appropriate tuning. With taper present the gravitational stiffness in the device is effectively

$$g' = gf(Z), \tag{107}$$

and this proves very useful when $f(Z) < 1$; that is, when some overall anti-taper has been incorporated.

13. Results and discussion

In figure 12 the ratio of capture width to duct diameter $C_W/2a$ is presented for aspect ratio $h/a = 1$, and different dimensionless tuning wavenumbers $\mu_0 = K_0 a = 0{\cdot}4$, 0·8, 1·2. For each tuning, the actual maximum of $C_W/2a$ is found at a wavenumber lower than the tuning wavenumber, but the values here are disappointing since $C_W/2a$ is nearly always less than one. It is possible to achieve higher values of $C_W/2a$ by tuning to wavenumbers that are smaller still, but figure 13 shows that the amplitudes of response in the duct necessary for such improved values become larger as μ_0 decreases, invalidating linear theory.

A rather different situation emerges on examining figures 14–17, representing results for smaller values of aspect ratio $\sigma = h/a = 0{\cdot}6$, 0·4. It is evident that as σ decreases the values of $C_W/2a$ improve, becoming closer to the maximum possible value $1/2\mu$ everywhere. There is an accompanying trend in the amplitude ratios which tend to increase if the tuning wavenumber is one of the larger values considered,

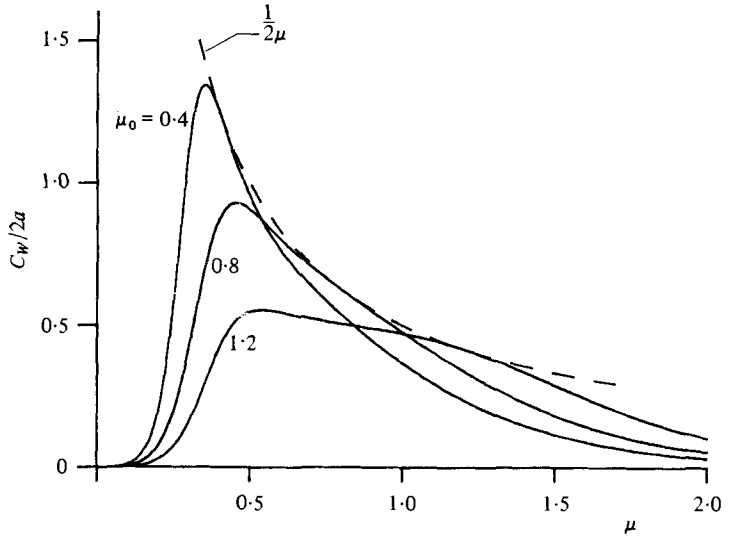

FIGURE 14. The capture width to duct diameter ratio plotted against dimensionless wavenumber $\mu = Ka$ for a duct of aspect ratio $\sigma = 0{\cdot}6$, for different values of tuning wavenumber $\mu_0 = K_0 a$. Dashed curve: the maximum capture width to diameter ratio $1/2\mu$.

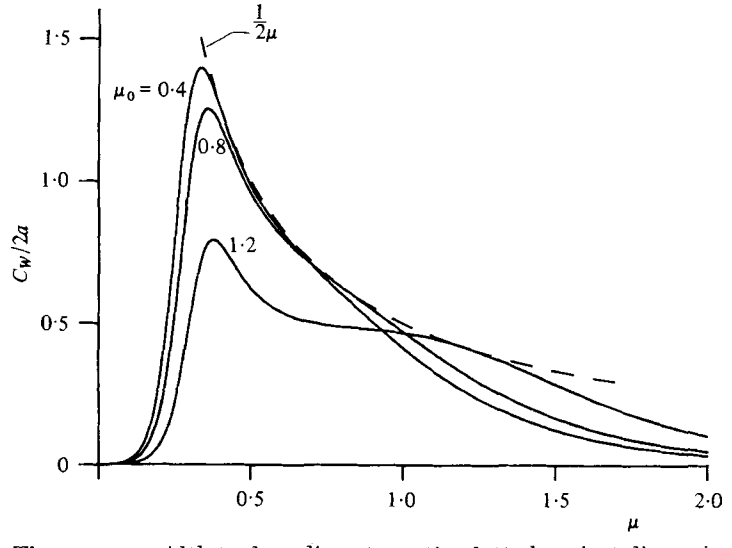

FIGURE 15. The capture width to duct diameter ratio plotted against dimensionless wavenumber $\mu = Ka$ for a duct of aspect ratio $\sigma = 0{\cdot}4$, for different values of tuning wavenumber $\mu_0 = K_0 a$. Dashed curve: the maximum capture width to diameter ratio $1/2\mu$.

but tend to decrease for $\mu_0 = 0{\cdot}4$; there is thus a 'cross-over' which occurs for σ about 0·5. It is surprising to note that when σ is less than about 0·3 (not shown) the greatest values of $C_W/2a$ are no longer given by the smallest tuning wavenumber; the drawback is, of course, the larger amplitude ratios.

The factor that prevents full advantage being taken of the small amplitude ratios

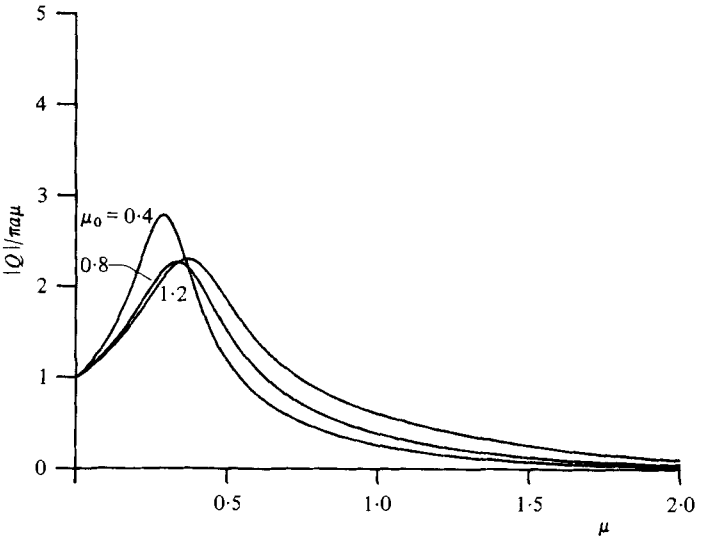

FIGURE 16. The amplitude ratio $|Q|/\pi a\mu$ plotted against dimensionless wavenumber $\mu = Ka$ for a duct of aspect ratio $\sigma = 0{\cdot}6$, for different values of tuning wavenumber $\mu_0 = K_0 a$.

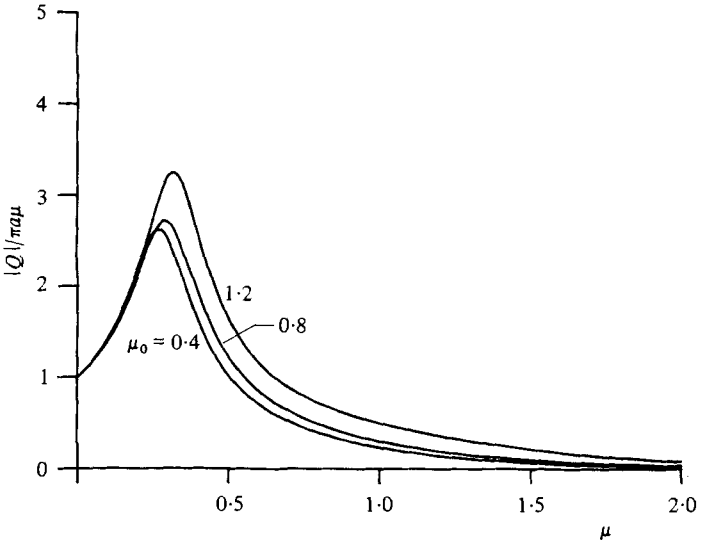

FIGURE 17. The amplitude ratio $|Q|/\pi a\mu$ plotted against dimensionless wavenumber $\mu = Ka$ for a duct of aspect ratio $\sigma = 0{\cdot}4$, for different values of tuning wavenumber $\mu_0 = K_0 a$.

and good performance, which occur when both σ and μ_0 are small, is the increasing steepness of the 'cut-off' at μ about 0·25. This is a result of the dominance of gravitational stiffness at low frequency, and is a major reason why the introduction of anti-taper in a real device could be beneficial. Figure 18 shows an example of this, for a duct where the air/water interface has 25 % greater area than the mouth. There is a reduction in amplitude ratio resulting from the greater area, but also an increase in bandwidth.

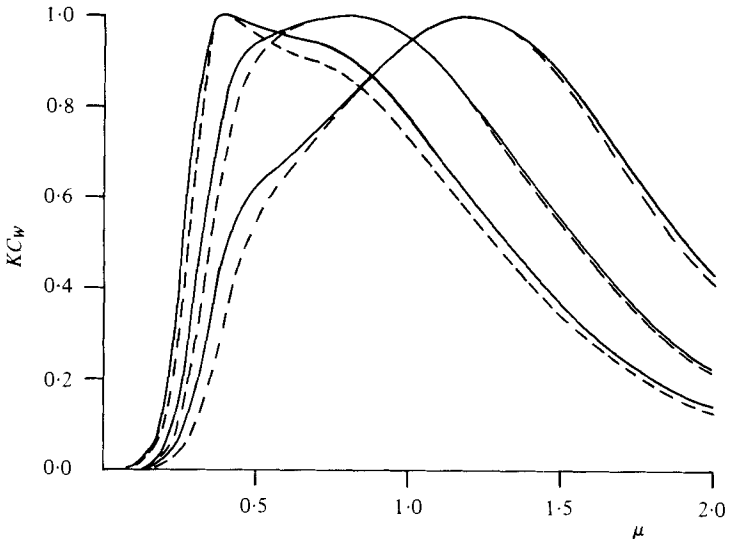

FIGURE 18. The capture width times wavenumber KC_W plotted against dimensionless wavenumber $\mu = Ka$ for a duct of aspect ratio $\sigma = 0{\cdot}6$, which is anti-tapered to reduce the amplitude ratios. Curves are shown for different values of the tuning wavenumber $\mu_0 = K_0 a$. Dashed lines: the corresponding results for a straight duct.

By contrast, the stiffness in the model of Thomas (1981) is a spring constant pertaining to the energy take-off mechanism, and this constant can be chosen to give resonance at a particular frequency when the duct length is fixed. This allows tuning at much lower wavenumbers, and hence produces greater values of capture width to duct diameter, than in the present case.

Another thing that becomes evident is that the value of duct length Z necessary to achieve the resonance condition (97a) is not, in general, strictly compatible with the implicit assumptions used in setting up the model. That is, in using the values of added mass and damping, derived for a straight duct, in the device of figure 1, it has been assumed that the U-bend and air/water interface are several duct radii below the mouth. This is not, however, in serious conflict with the results (which give Z/a around 1) since incorporating taper or anti-taper in the duct allows resonance to be chosen at a different design length.

It should be noted that the long-wavelength limit ($\mu \to 0$) is inappropriate for the assumptions of this analysis, that the sea bed and the lower duct were irrelevant when considering the device performance. In particular the amplitude ratio will not be unity at zero frequency, but will be some small positive quantity depending on the compressibility of the trapped air-column.

14. Conclusion

This paper has examined the Vickers twin oscillating water-column wave-energy device, modelling it as a single cylindrical duct. Linearized theory was used to set up the scattering and radiation problems. In part 1 the former problem was solved to high accuracy using a variational technique well suited to the simple boundary

conditions involved. This gave the pressure-amplification factor which was used in part 2 to yield the added mass and added damping from the radiation problem by means of a reciprocal theorem, which takes advantage of the linearization. The results presented in §11 have shown major qualitative differences between two- and three-dimensional ducts. This is particularly important in the added mass, which is large and variable (unlike that for two dimensions), and so helps to produce good band-widths.

Part 3 then derived the results for the capture width and amplitude ratio of the duct when absorbing energy, and curves of the device performance have been presented. It has been shown that, for certain aspect ratios and dimensionless tuning wavenumbers, it is possible for the duct to absorb energy over a crest length greater than its diameter, within the validity of linear theory.

Further work will consider a linear array of such devices interacting, since it has been shown in several recent theoretical and experimental investigations that the energy absorption characteristics of a device can be significantly enhanced by its mutual interaction with other devices.

I would like to thank Professor Sir James Lighthill for all the help and encouragement he has given me during this work, and also Dr D. V. Evans, Dr G. F. Knott and Mr H. J. Pearson for their advice and comments, and the Science Research Council for the financial support which made this research possible. I am also indebted to Mr J. R. Thomas for his co-operation in linking our two papers.

REFERENCES

ABRAMOWITZ, M. & STEGUN, I. 1964 *Handbook of Mathematical Functions.* Washington: National Bureau of Standards.

EVANS, D. V. 1976 *J. Fluid Mech.* **77**, 1–25.

EVANS, D. V. & MORRIS, C. A. N. 1972*a* *J. Inst. Math. Applics* **9**, 198–204.

EVANS, D. V. & MORRIS, C. A. N. 1972*b* *J. Inst. Math. Applics* **10**, 1–9.

GARRETT, C. J. R. 1970 *J. Fluid Mech.* **43**, 433–449.

HAVELOCK, T. H. 1929 *Phil. Mag.* **8** (7), 569–576.

KNOTT, G. F. & FLOWER, J. O. 1980 *J. Fluid Mech.* **100**, 225–236.

KOTIK, J. & MANGULIS, V. 1962 *Int. Shipbuilding Prog.* **9**, 361–368.

LIGHTHILL, M. J. 1979 *J. Fluid Mech.* **91**, 253–317.

MILES, J. W. 1967 *J. Fluid Mech.* **28**, 755–767.

MILES, J. W. 1971 *J. Fluid Mech.* **46**, 141–150.

NEWMAN, J. N. 1962 *J. Ship Res.* **6**, 10–17.

NOBLE, B. 1958 *Methods based on the Wiener–Hopf Technique.* Pergamon.

THOMAS, J. R. 1981 *J. Fluid Mech.* **104**, 189–215.

THORNE, R. C. 1953 *Proc. Camb. Phil. Soc.* **49**, 707–716.

URSELL, F. 1947 *Proc. Camb. Phil. Soc.* **43**, 374–382.